Contrib Mineral Petrol (2007) 154:171–190
DOI 10.1007/s00410-007-0185-9

ORIGINAL PAPER

Distribution of platinum-group elements in the Platreef at Overysel, northern Bushveld Complex: a combined PGM and LA-ICP-MS study

D. A. Holwell · I. McDonald

Received: 26 July 2006 / Accepted: 25 January 2007 / Published online: 10 February 2007

Abstract Detailed mineralogical and laser ablation-inductively coupled plasma-mass spectrometry studies have revealed the physical manifestation of the platinum-group elements (PGE) within the Platreef at Overysel, northern Bushveld Complex, South Africa. The PGE in the Platreef were originally concentrated in an immiscible sulfide liquid along with semi-metals such as Bi and Te. As the sulfide liquid began to crystallize, virtually all the Os, Ir, Ru and Rh partitioned into monosulfide solid solution (mss), which on further cooling, exsolved to form pyrrhotite and pentlandite with Os, Ir and Ru remaining in solid solution in both phases with Rh prefentially partitioning into pentlandite. Platinum, some Pd and Au were concentrated in the residual sulfide liquid after mss crystallization, and were then concentrated in an immiscible late stage melt along with semi metals, which was expelled to the grain boundaries during crystallization of intermediate solid solution (iss) to form Pt and Pd tellurides and electrum around the margins of the sulfide grains. Tiny droplets of this melt trapped in the crystallizing mss and iss cooled to form Pt–Bi–Te microinclusions in all sulfide phases, whilst the excess Pd was accommodated in solid solution in pentlandite. Minor redistribution and recrystallization by hydrothermal fluids occurred around xenoliths and at the very base of the mineralized zone within the footwall, however, the overall lack of secondary alteration coupled with the volatile-poor nature of the gneissic footwall have allowed the preservation of what may be the most 'primary' style of Platreef mineralization. The lack of PGM inclusions within early liquidus phases suggests very early sulfur saturation in the Platreef, lending support to theories involving S saturation occurring prior to intrusion of the Platreef, possibly within a staging chamber.

Keywords Platreef · Bushveld Complex · Platinum-group minerals · Platinum-group elements · Sulfide minerals · Laser-ablation ICP-MS

Communicated by T.L. Grove.

D. A. Holwell (✉) · I. McDonald
School of Earth, Ocean and Planetary Sciences,
Cardiff University, Main Building, Park Place,
Cardiff CF10 3YE, UK
e-mail: HolwellDA@cf.ac.uk

Introduction

The Bushveld Complex in South Africa is the World's largest layered igneous intrusion, made up of a 7–8 km thick sequence of mafic and ultramafic lithologies covering an area of 65,000 km^2 (Eales and Cawthorn 1996). It is the largest repository of magmatic ore deposits on Earth and contains around 75% of the World's resources of platinum-group elements in three main deposits: the UG2 chromitite, the Merensky Reef and the Platreef (Kendall 2006). The Platreef is a 10–400 m thick unit of pyroxenitic lithologies with platinum-group element (PGE) and base-metal sulfide (BMS) mineralization located in the northern limb of the Complex (Kinnaird and McDonald 2005). North from the town of Mokopane, the Platreef forms the base of the Bushveld layered igneous sequence and rests unconformably upon a succession of progressively older sedimentary units of the late Archaean—early

Proterozoic Transvaal Supergroup, and Archaean basement. Northwards from Mokopane, these footwall units are comprized of: quartzites and shales of the Timeball Hill Formation; shales of the Duitschland Formation; the Penge banded iron formation; the Malmani Subgroup dolomites and, north from the farm Zwartfontein, Archaean basement granites and gneisses, which form the footwall on the farm Overysel. The Platreef is overlain by norites and gabbronorites generally assigned to the Main Zone of the Complex (Fig. 1).

The increase in exploration and mining activity in recent years has facilitated an expanding number of studies to be undertaken on the Platreef, including detailed mineralogical studies of the platinum-group minerals (PGM) by Armitage et al. (2002) and Holwell et al. (2006) at Sandsloot, where the footwall is Malmani Subgroup, and by Hutchinson and Kinnaird (2005) at Macalacaskop and Turfspruit, where the floor rocks are Duitschland Formation. These studies have highlighted the differences in PGM mineralogy at localities along strike where the interaction of the Platreef magma with different floor rock lithologies appears to have had an important influence on the resulting PGM mineralogy. This study provides the first detailed investigation into the PGM at a locality where Archaean granites and gneisses form the floor and follows up the petrological and geochemical investigation into the Platreef at Overysel by Holwell and McDonald (2006).

This study is also the first laser ablation-inductively coupled plasma-mass spectrometry (LA-ICP-MS) study into the PGE contents of BMS to be combined with PGM studies in order to investigate the physical manifestation of the PGE in the Platreef. The purpose of this is to constrain where each of the PGE reside in relation to sufide minerals, data which is important both scientifically, as it reveals important information regarding the processes involved in noble metal enrichment and sulfide liquid fractionation in Ni–Cu–PGE deposits, and economically in terms of grade distribution and mineral processing.

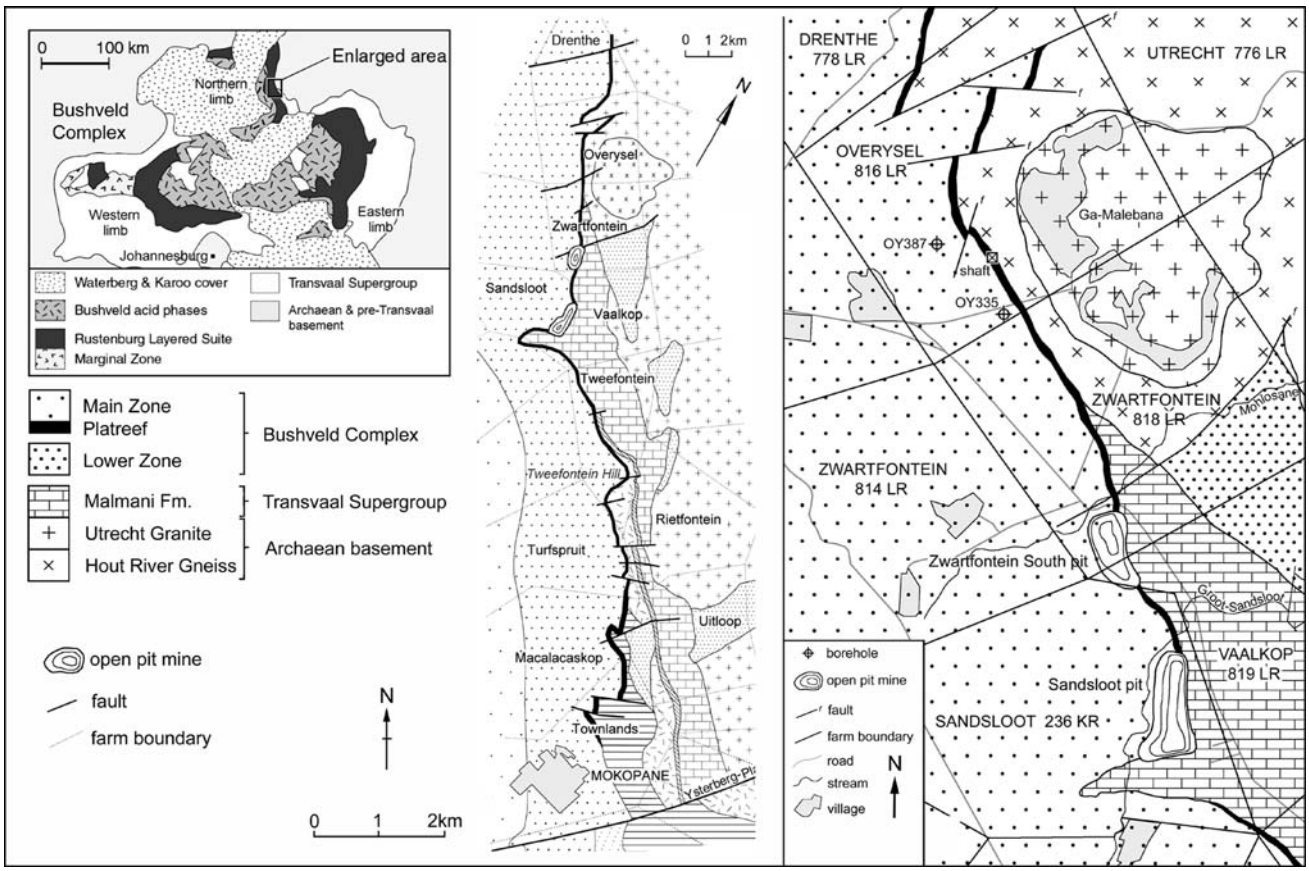

Fig. 1 Geological map of the Platreef, showing the locality of boreholes OY335 and OY387, the 1980 shaft and farms referred to in the text. Based on field mapping and published maps of the Geological Survey of South Africa (Council for Geoscience 1995)

Samples and methods

We utilize the same samples as Holwell and McDonald (2006), where the sampling procedure is described. Two borehole cores drilled on the farm Overysel were sampled: borehole OY335 which intersects a 95 m thick package of pyroxenites with several xenoliths and a 20 m thick package of footwall gneisses; and borehole OY387, which comprises a 25 m thick, continuous package of pyroxenites and 117 m of gneiss with zones of mineralization extending well into the footwall. Both holes intersect granite at depth. The locality of the boreholes are shown in Fig. 1. Sample numbers refer to depth, but do not reflect true thickness, with dips around 45°. Stratigraphic logs of the two cores are shown in Fig. 2, together with the position of the samples. Additional grab samples of chromitite were obtained from the dumps at the disused exploration shaft, sunk in 1980 on the farm, near the village of Ga-Melebana (Fig. 1).

Laser-ablation-ICP-MS on sulfides was carried out using a New Wave Research UP213 UV laser system coupled to a Thermo X Series ICP-MS at Cardiff University. The isotopes ^{33}S, ^{59}Co, ^{61}Ni, ^{65}Cu and ^{66}Zn were detected to monitor the composition of the sulfides together with the precious metal isotopes ^{99}Ru, ^{101}Ru, ^{103}Rh, ^{105}Pd, ^{106}Pd, ^{189}Os, ^{193}Ir, ^{195}Pt and ^{197}Au. The isotopes of the semi metals ^{75}As, ^{82}Se, ^{125}Te, ^{121}Sb, and ^{209}Bi were also analyzed as these elements commonly form PGM, and are used to distinguish if a particular PGE in a sulfide is present within solid solution, or as a PGM phase. Full details of the analytical conditions and standards are described in McDonald (2005). Platinum-group minerals were analyzed at Cardiff University using a Cambridge Instruments LEO S360 scanning electron microscope, coupled to an Oxford Instruments INCA energy dispersive X-ray analysis system.

Petrology and mineralogy

The petrology of cores OY387 and OY335 have been described in detail in Holwell and McDonald (2006), and only a brief overview of the most salient features is given here.

Footwall lithologies

The footwall at Overysel is made up of Hout River Gneiss and Utrecht Granite. The gneisses are banded granulites comprizing pale, quartzo-feldspathic bands and darker, orthopyroxene-rich bands. They contain a restricted, anhydrous mineralogy of quartz, oligoclase and orthopyroxene ($En_{70–75}$). Base metal sulfides occur sporadically in the gneisses and typically occur as small blebs at grain boundaries between host silicates. In places, the sulfide content of the rock can become very high, with both net-textured and massive sulfides present in the OY387 core at around 380 m depth (Fig. 2). Sulfide blebs are typically made up of pyrrhotite, with pentlandite around the margins and chalcopyrite either at the margins or as laths within pyrrhotite. The gneisses are intruded by granitic dykes. The gneisses adjacent to these are pervasively altered by hydrous minerals such as amphiboles and chlorite. Borehole OY387 also intersects a 3 m thick zone of pyroxenite deep into the gneisses (sample OY387–384), which is of Lower Zone affinity. The Utrecht granite is a pink, fine- to medium-grained granite consisting of mesoperthitic alkali feldspar, quartz and minor muscovite. Where mineralized, the rock has a bleached appearance and contains some secondary amphiboles and micas, with chalcopyrite and millerite the most common sulfides.

Igneous Platreef lithologies

The pyroxenites are typically medium- to coarse-grained and made up of cumulus orthopyroxene ($En_{75–80}$), 5–20% intercumulus plagioclase, up to 5% clinopyroxene and a little quartz, with some accessory phlogopite, chromite and ilmenite. Quartz becomes more common with depth, and is indicative of an increasing amount of contamination from a felsic melt derived from partial melting of the footwall gneisses. Alteration by micas and carbonates occurs sporadically. Sulfides occur within the interstitial assemblage as blebs, made up of a pyrrhotite core, with pentlandite and chalcopyrite margins, and are commonly <10 mm and make up <3% of the total modal assemblage. Chromitites are present in both cores as small, angular xenoliths within the feldspathic pyroxenites. Chromitite bodies also occur, and the exploration mining (described by White 1994), encountered some large but discontinous chromitite bodies. Samples of chromitite taken from the dumps at the disused shaft are irregular and discontinuous, up to 30 cm thick and contain some pentlandite, with rarer chalcopyrite. Xenoliths of calc-silicate up to 10 m thick are also present in the OY335 core, some of which are serpentinized (Fig. 2), and containing abundant metamorphic olivine and clinopyroxene, with some orthopyroxene, amphibole and BMS. The

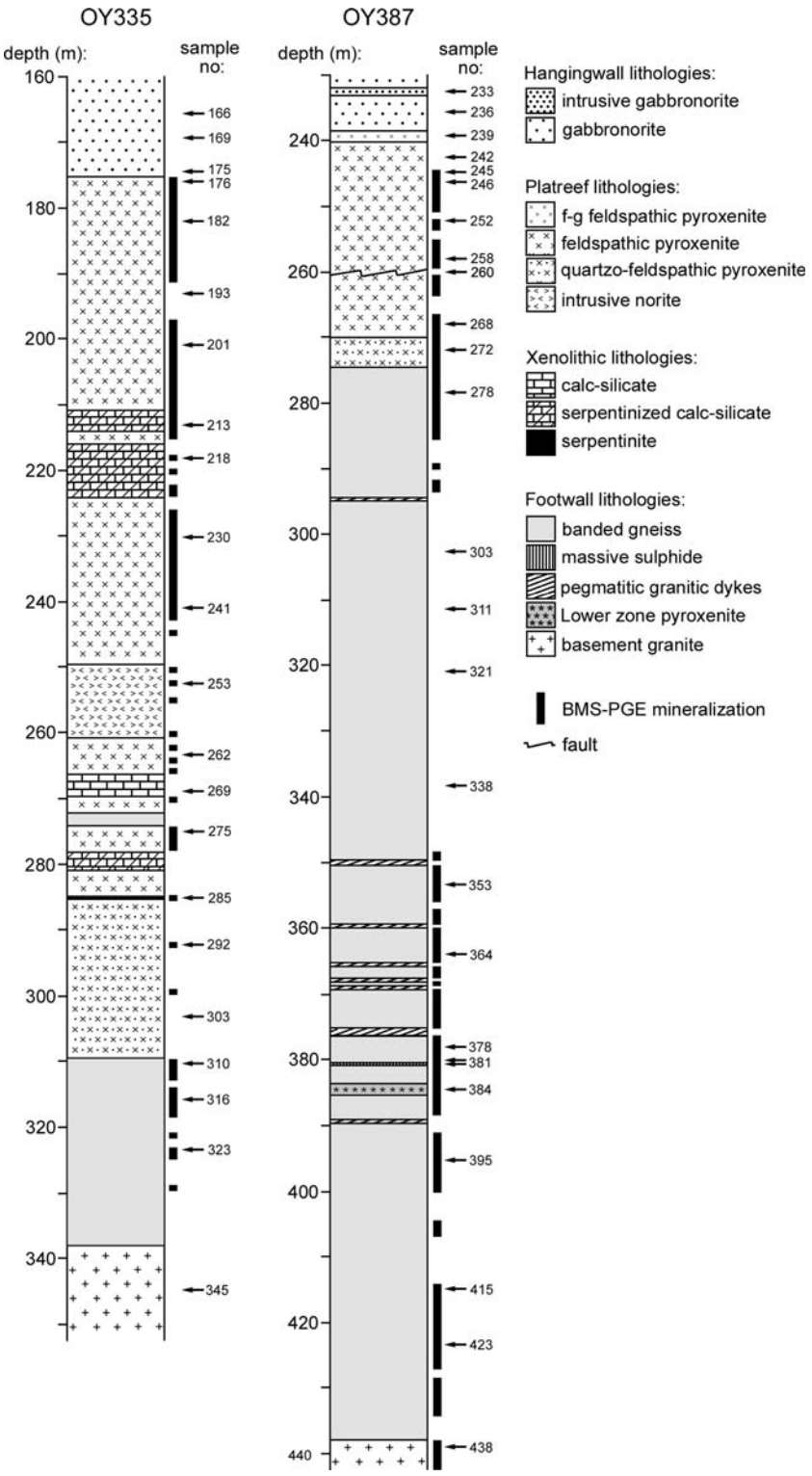

Fig. 2 Statigraphic logs of borehole cores OY335 and OY387 showing the positions of the samples and zones of visible BMS–PGE mineralization

overlying hangingwall rocks are made up of gabbronorites comprising 40–80% cumulus plagioclase, with cumulus and intercumulus orthopyroxene and oikocrystic clinopyroxene.

PGE mineralization

Holwell and McDonald (2006) identified a number of features of the PGE mineralization at Overysel, many

of which were unique to the locality and can be summarized as follows:

1. PGE mineralization within the two cores mirrors the presence and abundance of BMS.
2. Pt/Pd ratios are consistently around 0.7–0.8 and Pt/Au ratios are around 7–8 throughout both the Platreef and the footwall.
3. With depth into the footwall, progressive fractionation of the PGE is observed. This is seen in the sloping profile (Pt + Pd)/(Ir + Ru), which increases by several orders of magnitude with depth into the footwall, with strong depletions in Ir, Ru and Rh observed on normalized plots.
4. PGE were transported into the footwall gneisses within a fractionating sulfide liquid that percolated down through an interconnected, inter-granular melt network. This is in contrast to the calc-silicate floor at Sandsloot, where the main mechanism for transport of PGE into the footwall is believed to be within a hydrothermal fluid.
5. The millerite and chalcopyrite-rich assemblage in the bleached granite at the base of the gneisses in core OY387 is a hydrothermal assemblage, possibly formed by the expulsion of a fluid from the final stages of the evolving sulfide liquid.

In light of these discoveries, particularly the strong PGE–BMS relationships, this study builds upon them by investigating the way in which the PGE mineralization has manifested itself in terms of the platinum-group mineralogy and the role of BMS as hosts for PGE.

Platinum group mineralogy

Forty-three polished thin sections and blocks from the Platreef, xenoliths therein and the footwall from the two borehole cores, along with underground chromitite samples obtained from the dumps were examined for PGM on the SEM. More than 750 individual PGM grains were identified and are listed in Table 1. The PGM identified were grouped as: (1) Pt/Pd sulfides, (2) other PGE sulfides, (3) Pt/Pd tellurides, (4) Pt/Pd arsenides, (5) Pt/Pd antimonides, (6) Pt/Pd bismuthides, (7) PGE sulfarsenides, (8) Pt/Pd alloys with Fe, Cu, Sn, Pb, and (9) Au- and Ag-bearing minerals. Each occurrence was also classified by its textural association and by its size.

Grain size and relative grain area

Each PGM grain's long and short axes were measured in micrometres. Relative proportions of the various PGM species type are based on an estimation of area (and by inference, volume) of each grain. Using the long and short axis dimensions, the area of each grain was approximated to the area of an ellipse around the two axes, in the manner described in Holwell et al. (2006) for PGM at Sandsloot. This produces data that accurately reflect the relative proportions of each PGM type within an assemblage, and is directly comparable to the Sandsloot database in Holwell et al. (2006). This method of data presentation is preferable to proportions of PGM type by number of grains, which can give erroneous significance to large numbers of very small grains.

Assemblages

The PGM assemblage in each lithology is shown in Table 2 and the textural associations of the PGM within each lithology are shown in Table 3. The vast majority are Pt and Pd phases and the most common types of PGM are Pt and Pd tellurides, which make up 46% of all PGM identified (Table 2). Platinum arsenides, exclusively in the form of sperrylite ($PtAs_2$), and Pt sulfides (mostly cooperite, PtS) are common and Pt and Pd bismuthides are also important. Alloys, antimonides and sulfarsenides are minor phases. In detail, PGM assemblages vary with host rock lithology.

The PGM assemblage within the reef feldspathic pyroxenites is overwhelmingly dominated by Pt tellurides, most of which also contain some Bi in place of Te, for example, most moncheites have the formula $Pt(Te,Bi)_2$. Ni tellurides are absent from the assemblage and no Ni is present in solid solution within the Pt/Pd telluride phases. Sulfides and alloys are present, but rare. Although 7.5% of the assemblage by area is comprised of Pd alloys (Table 2), it can be seen from Table 1 that this contribution is skewed by a single, though large, grain of atokite (Pd_3Sn). Electrum (Au,Ag) is common and makes up 22% of the whole assemblage. Most PGM grains are associated with BMS, although very few are actually included within BMS grains, and most occur either as grains at the contact between BMS and silicate phases or within silicate phases as satellite grains around BMS (Fig. 3a, b; Table 3). Where alteration of the reef pyroxenite by sericite and carbonates has taken place, there is a decrease in the proportion of telluride PGM phases, and a corresponding relative increase in sulfides. Sobolevskite (PdBi) is very common, although the grains are very small and the proportion by area is minimal. The spatial associations are highly comparable to those in the unaltered reef.

The chromitites contain a very distinctive PGM assemblage, dominated by laurite and the sulfarsenides

Table 1 List of all PGM identified, together with ideal formulae, and number of occurrences within the lithologies in the Overysel cores

Name	Ideal formula	RFP	ARP	CHR	CQP	CSX	GS	AGS	NTS	MS	LZP	BGT	Total
Moncheite	$PtTe_2$	50	21				47	9	38	101	2	4	272
Kotulskite	PdTe	10	16	7		1	39	5		3			81
Sobolevskite	PdBi	1	11	14	1	5	14				1	14	61
Electrum	Au–Ag	15	9			1	16	2		2		4	49
Sperrylite	$PtAs_2$	5	11	7		9	4	3		2	1	4	46
Cooperite	PtS	4	16	8	4		8	4		1			45
Michenerite	PdTeBi	2	7	8			10	1		3	1	2	34
Froodite	$PdBi_2$	2	1				13	2			5	5	28
Merenskyite	$PdTe_2$	5	3			5	7	1	4				25
Hollingworthite	RhAsS			10		6							16
Unnamed	Pd(Bi,Sb)					13							13
Laurite	RuS_2			11									11
Maslovite	PtTeBi							2		6	1		9
Platarsite	PtAsS			7		1							8
Insizawaite	$PtBi_2$		1	1			2	1			2	1	8
Hessite	Ag_2Te	2				1	1					3	7
Stibiopalladinite	Pd_5Sb_2					1	3	1					5
Unnamed	$PtCuBiS_3$						1					4	5
Paolovite	Pd_2Sn		4				1						5
Atokite	Pd_3Sn	1	1				2						4
Crerarite	$(Pt,Pb)Bi_3S_4$						4						4
Unconstrained	Pt–Pd–Te–Bi	2						1					3
Palarstenide	$Pd_5(Sn,As)_2$		3										3
Rustenburgite	Pt_3Sn	2			1								3
Unconstrained	Pd–Pt–Te						2						2
unconstrained	Bi–Pb–Pt–Cu–Bi–S										1	1	2
Pd–melonite	$(Ni,Pd)Te_2$	1											1
Unconstrained	Pt–As–Te–Bi		1										1
Unconstrained	Pd–Pt–Te–Bi–As		1										1
Native silver	Ag						1						1
Unconstrained	Pt–Cu–Bi–Te						1						1
Palladian gold	Au–Pd						1						1
Braggite	(Pt,Pd)S						1						1
Argentite	Ag_2S						1						1
Unconstrained	Pt–Pd–Cu–Bi–S							1					1
Unnamed	$(Pt,Cu,Rh,Ir)_2S_3$			1									1
Unnamed	PdPtBi			1									1
Unnamed	Ag_4S											1	1

RFP reef feldspathic pyroxenite, *ARP* altered reef feldspathic pyroxenite, *CHR* chromitite, *CSX* calc-silicate xenoliths, *CQP* chromitiferous quartzo-feldspathic pyroxenite, *GS* gneiss, *AGS* amphibolitic gneiss, *NTS* net-textured sulfides, *MS* massive sulfides, *LZP* gneiss-hosted Lower Zone pyroxenite, *BGT* basement granite

solid solution series hollingworthite–platarsite (RhAsS–PtAsS). The major carrier of Pd is sobolevskite–kotulskite solid solution, Pd(Bi,Te), which contains almost equal atomic proportions of Bi and Te. This is the only lithology, which contains any significant discreet Rh phases and is the sole lithology to contain any Ru- or Ir-bearing PGM. Laurite is occasionally Ir-bearing, hollingworthite and platarsite are usually Ir- and Ru-bearing and Rh-bearing sperrylite is also common. Most of the Pd-bearing phases are silicate-hosted and only 20% of all grains are located at the boundary between silicates and small sulfide (almost exclusively pentlandite) grains within the silicate matrix. In Table 3, the 'oxide' associations refer to PGM in contact with chromite grains, which was the most common occurrence for laurite. Two PGM grains, one laurite and one cooperite, were found as inclusions within chromites. In the chromitiferous quartzo-feldspathic pyroxenite, only six PGM were found, which were dominated by the sulfide cooperite, rather than laurite. No PGM were found as inclusions in the chromites in this lithology.

The PGM assemblage in the serpentinized calc-silicate xenoliths is the most arsenide dominant in the whole sample suite, with 82% sperrylite by area. Palladium tellurides are the next most common PGM type. There are also several smaller grains of the Pd bismuthides sobolevskite and an unnamed phase

Table 2 Proportions of PGM type within each lithology in the Overysel cores, in percentage of the total area of 100% PGM

PGM type	RFP	ARP	CHR	CQP	CSX	GS	AGS	NTS	MS	LZP	BGT	ALL
Pt sulfides	4.3	64.9	8.4	92.2		18.7	17.9		2.5		5.4	13.4
Other PGE sulfides			30.8									0.6
Pt tellurides	51.3	8.1				17.5	29.2	97.3	88.5	1.3	12.9	25.5
Pd tellurides	13.2	18.5	19.1		10.4	49.2	4.0	2.7	3.3	1.0	0.5	20.8
Pt arsenides	1.1	2.5	7.9		86.2	5.7	3.8		5.0	0.1	1.6	16.7
Pd antimonides					0.5	0.4	0.4					0.2
Pt bismuthides		0.2	0.5			0.1	0.1			82.7	2.9	5.9
Pd bismuthides	0.4	1.7	9.1	3.9	2.1	4.7	0.7			14.9	30.9	5.9
PGE sulfarsenides			24.2		0.7							0.6
Pt dominant alloys	0.3			3.9								<0.1
Pd dominant alloys	7.5	1.8				0.8						0.9
Au/Ag minerals	21.9	2.3			0.1	2.9	43.9		0.7		45.8	9.5

For lithology abbreviations, see Table 1

ALL all PGM in all lithologies

Table 3 Associations of all PGM and Au, Ag phases, Pt dominant phases only, and Pd dominant phases only within each lithology in the Overysel cores in percentage of the number of grains

Association	RFP	ARP	CHR	CQP	CSX	GS	AGS	NTS	MS	LZP	BGT
All PGM, Au, Ag phases											
Sulfide	2.6	8.6	4.0			6.2	15.6	9.5	83.1	21.4	4.8
Sulfide/silicate	28.1	37.1	20.0	66.6	59.5	48.0	50.0	81.0	11.0	42.9	21.4
Primary silicate	45.6	28.6	36.0	16.7	16.7	32.8	21.9	9.5	5.9	14.3	73.8
Secondary silicate	23.7	25.7	21.3		23.8	13.0	12.5			21.4	
Oxide			18.7	16.7							
Pt-dominant											
Sulfide	4.0	11.9	4.2			6.8	23.8	10.5	87.3	14.3	
Sulfide/silicate	29.0	35.7	20.8	60.0		60.3	38.1	81.6	10.9	28.6	14.3
Primary silicate	46.0	38.1	41.7	20.0	55.6	27.4	28.6	7.9	1.8	14.3	85.7
Secondary silicate	21.0	14.3	16.6		44.4	5.5	9.5			42.8	
Oxide			16.6	20.0							
Pd-dominant											
Sulfide	8.7	5.4	3.5			3.6				28.6	
Sulfide/silicate	39.1	38.2	27.6	100.0	61.3	39.5	80.0	75.0	16.7	57.1	20.0
Primary silicate	34.8	21.8	24.1		3.2	39.5	10.0	25.0	83.3	14.3	80.0
Secondary silicate	17.4	34.6	31.0		35.5	17.4	10.0				
Oxide			13.8								

For lithology abbreviations, see Table 1

Pd(Bi,Sb). This is the only rock type, other than the chromitites, in which a few sulfarsenides are present, mainly hollingworthite (RhAsS). The associations of the PGM within this assemblage differ from all the others in that it is the Pd phases, which show a distinct association with BMS over Pt phases, with all the Pt minerals enclosed within silicates.

The gneisses have a similar assemblage to that of the reef pyroxenites. Tellurides dominate, although unlike in the pyroxenites, Pd phases are more common than moncheite. Sulfides [cooperite, crerarite: $(Pt,Pb)Bi_3S_4$, and a single grain of braggite (Pt,Pd)S] make up 18.7% of the assemblage. All PGM were spatially associated with BMS and most grains were found at the sulfide–silicate contact (Fig. 3c, Table 3). Altered, or amphibolitic, gneisses are dominated by a few large grains of electrum, with the remainder of the assemblage more Pt-dominant than the rest of the gneiss. The associations were similar to the unaltered gneiss, though only Pt phases were observed as inclusions within BMS, and the majority of Pd phases were located at the sulfide–silicate contact.

The net-textured and massive sulfides within the gneisses are overwhelmingly dominated by tellurides, most of which also contain some Bi. Indeed, the net-textured sulfide sample contained no other type of PGM, with 97% of the grains being moncheite, and the remainder merenskyite. Virtually all grains were located around the sulfide margins in the net-textured sulfide, and only Pt minerals were found as inclusions

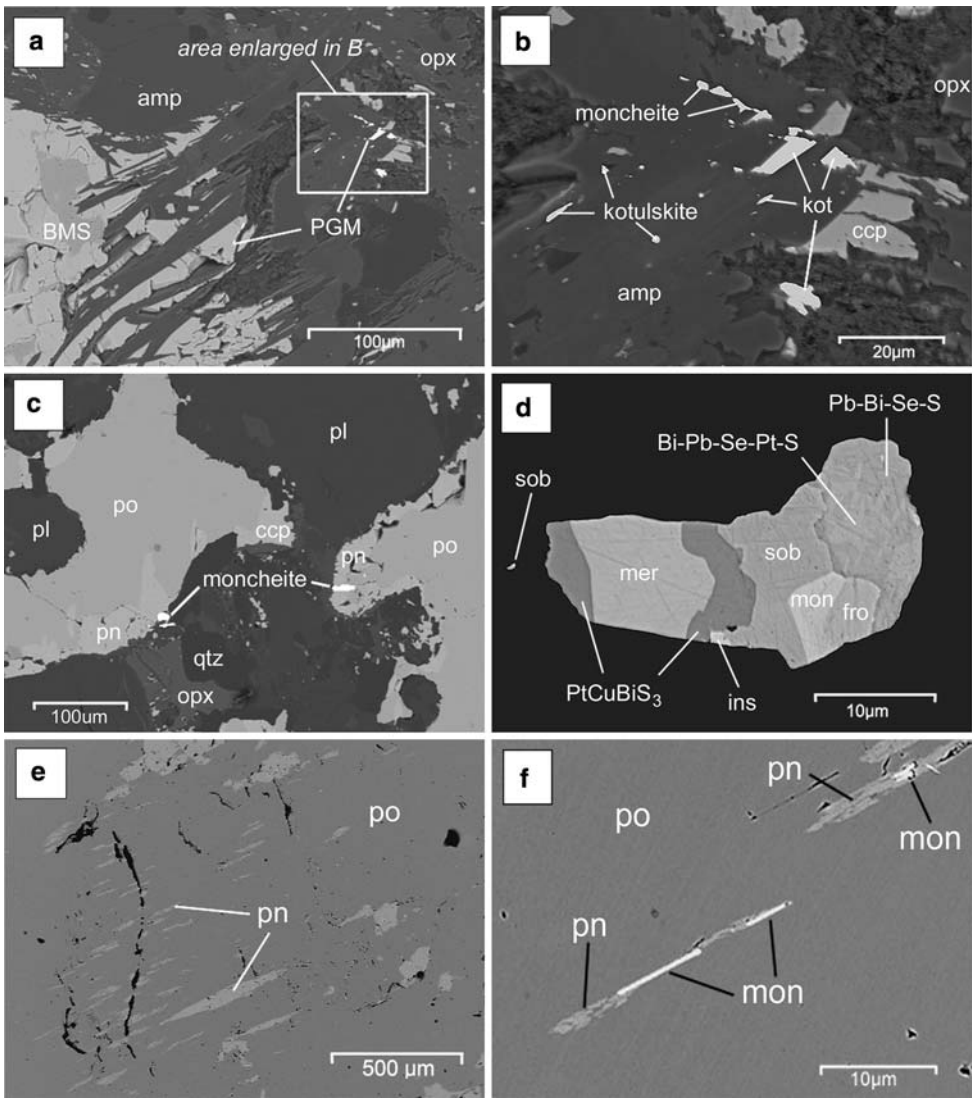

Fig. 3 Backscattered scanning electron micrographs of **a** typical association of PGM at the contact between BMS and silicates, and as satellite grains in close proximity to the BMS grain, enclosed within secondary amphiboles (*amp*) between the BMS and primary silicates such as orthopyroxene (*opx*). **b** Enlarged area from A, showing grains of moncheite (*mon*) and kotulskite (*kot*) and remnant chalcopyrite (*ccp*) enclosed in secondary amphibole. **c** Typical association of PGM (*moncheite*) located at the edge of BMS grains made up of pyrrhotite (*po*), pentlandite (*pn*) and chalcopyrite (*ccp*) within footwall gneiss composed of quartz (*qtz*), plagioclase (*plag*) and orthopyroxene (*opx*). **d** Polyphase PGM enclosed within quartz in mineralized basement granite, containing sobolevskite (*sob*), the unnamed $PtCuBiS_3$, merenskyite (*mer*), insizawite (*ins*), moncheite (*mon*), froodite (*fro*), and two intergrown, unconstrained Pb–Bi–Se–S phases, one of which is Pt-bearing. **e** Exsolution lamellae of pentlandite within pyrrhotite in a sample of massive sulfide. **f** Enlarged view of massive sulfide showing the association of moncheite with exsolved pentlandite within pyrrhotite

in the sulfides. The massive sulfide contained a few sulfides, arsenides and electrum, although was still made up of 88% Pt tellurides (Table 2). The majority of the Pt phases were included within BMS, with the remainder being located at the contact between BMS and silicate phases. The Pd phases were almost all concentrated along the edge of the massive sulfide zone and included within silicates. Many of the moncheite grains appear to be exsolved, along with pentlandite, out of pyrrhotite. Figure 3e and f show the preferred orientation of pentlandite and moncheite exsolved from pyrrhotite, with moncheite typically rimmed by pentlandite in such textural relationships.

The mafic Lower Zone-like pyroxenite intersected within the lower gneiss in borehole OY387 has an assemblage dominated by bismuthides, particularly insizawite ($PtBi_2$) and froodite ($PdBi_2$). No Au minerals were found. The BMS in this lithology were dominated by chalcopyrite.

Some BMS and PGE mineralization was identified in the sample of altered basement granite. The assemblage in the altered and mineralized basement granite contained 46% Au and Ag minerals by area, with the true PGM assemblage being dominated by the Pd bismuthides sobolevskite and froodite. Moncheite and the unnamed bismutho-sulfide $PtCuBiS_3$ were also common. A complex polyphase grain of bismuthides, tellurides and $PtCuBiS_3$ from a sample of granite is shown in Fig. 3d. The majority of PGM found were included in primary silicates, with only electrum occurring as inclusions in BMS. The BMS phases in this lithology are dominated by chalcopyrite and millerite (NiS).

LA-ICP-MS analysis

A prominent finding of this and other recent investigations into the PGE mineralogy within the Platreef (e.g., Armitage et al. 2002; Hutchinson and Kinnaird 2005; Holwell et al. 2006) is that the vast majority of PGM, are Pt and Pd phases. The failure to locate enough PGM to account for the observed whole rock contents of Rh, Ru, Ir and Os, particularly in the Platreef pyroxenites, indicates that these elements are likely to be present in trace concentrations in other minerals; most likely in solid solution within BMS. Ore microscopy studies and SEM-based analyses are not sufficient for detecting trace levels of PGE within sulfide minerals. Laser-ablation ICP-MS (LA-ICP-MS) techniques are the most precise way of achieving detection to such low levels as tens of parts per billion, which is one to three orders of magnitude greater than can be achieved by other in situ techniques such as micro-Proton Induced X-ray Emission (micro-PIXE) and Secondary Ion Mass Spectrometry (SIMS) (Cabri et al. 2003). We performed a series of LA-ICP-MS analyses on a number of sulfide phases from the Platreef feldspathic pyroxenites, chromitites and the basement gneisses at Overysel, together with a few samples of Platreef feldspathic pyroxenite from Sandsloot for an along-strike comparison. The results of the analyses are shown in Table 4 and the results from the Platreef pyroxenites are also plotted in Fig. 4. A selection of time resolved analysis (TRA) spectra are shown in Fig. 5 to illustrate the most important features.

PGE contents of BMS and other phases

Platreef feldspathic pyroxenites

From Table 4, it can be seen that pyrrhotite is the major carrier of Os, Ir and Ru, holding on average 1 ppm Os, 2 ppm Ir and 8 ppm Ru, and the standard deviations show that the values are highly consistent both within and between samples. Figure 4a and b show a high degree of correlation between these elements in pyrrhotite. Some grains held minor amounts of Rh, but no appreciable Pd was present in any of the pyrrhotites (Fig. 4d). There is a positive correlation between the IPGE and Ni contents in pyrrhotite, which is illustrated in Fig. 4e. However, different slopes are evident at different locations, with the Sandsloot samples showing a higher PGE/Ni ratio than those found at Overysel. Figure 5a shows a TRA spectrum for a pyrrhotite grain from the Platreef pyroxenites, with smooth, parallel patterns of Ru, Ir and Os with S, indicating the IPGE are present in solid solution in the pyrrhotite.

Pentlandite was also found to contain concentrations of the IPGE with similarly high degrees of correlation between these elements (Fig. 4a, b). Their concentrations, however, are consistently lower than those in pyrrhotite (Table 4, Fig. 4a, b), with pyrrhotite, on average, hosting 1.5 times as much IPGE than pentlandite in the Overysel samples. This is not a consistent relationship however, with the two samples from Sandsloot showing opposite trends (Table 4). Pentlandite is the major carrier of Rh and Pd, containing on average 15 ppm Rh and 119 ppm Pd in the Overysel pyroxenites. Concentrations of Rh and Pd within individual pentlandite crystals are quite variable and high Rh contents do not necessarily correlate with high Pd contents (Fig. 4f). Both Rh and Pd show poor correlations with the IPGE (Fig. 4c, d). Some minor Pt (<0.2 ppm) is apparently present in solid solution in a few pentlandite analyses, one example of which is shown in Fig. 5b, which demonstrates smooth profiles for all PGE, with particularly high abundances of Rh and Pd which mirror Ni and S, thus confirming their presence in solid solution.

No PGE were present in solid solution within chalcopyrite, however, some Pt (with correspondingly high Bi and occasionally Te concentrations) was detected that did not mirror base metal concentrations. The TRA spectrum for one of these examples is shown in Fig. 5c where Pt and some trace Pd, rather than mirroring the S and base metal contents, show distinct peaks along with Bi. In these relationships, Pt appears to be present as discreet, micrometer to sub-micrometer PGM inclusions, rather than in solid solution in the sulfide. Further examples are also present in the TRA spectra shown in Fig. 5d and f and they are present in all of the major sulfide phases. It is worth noting that we analyzed for the semi-metals As, Sb, Te, Bi and Se, all of which form PGM, but only Pt(±Pd)–Bi(±Te) phases were detected as microinclusions.

Table 4 Compositions of base metal sulfides from the Platreef at Overysel and Sandsloot as determined by LA-ICP-MS analysis

	S (wt%)	Co (ppm)	Ni (wt%)	Cu (wt%)	Os (ppm)	Ir (ppm)	Ru (ppm)	Rh (ppm)	Pt (ppm)	Pd (ppm)	Au (ppm)	Te (ppm)	Bi (ppm)
Overysel Reef pyroxenites													
Pyrrhotite (n = 8)													
Mean	38.7	22.8	0.51	0.00	0.93	1.80	7.81	0.45	0.61	0.06	0.00	1.64	0.92
σ	1.7	12.1	0.13	0.00	0.11	0.34	2.31	0.55	0.59	0.04	0.00	0.87	0.64
Max	40.1	41.7	0.71	0.01	1.05	2.32	11.6	1.59	1.74	0.11	0.01	2.60	1.52
Min	34.6	9.0	0.34	BDL	0.76	1.29	4.17	0.01	0.01	BDL	BDL	BDL	BDL
Pentlandite (n = 8)													
Mean	33.7	2,969	34.4	0.02	0.59	1.20	5.16	15.0	0.45	119	0.00	1.49	0.85
σ	0.4	1,653	5.6	0.05	0.22	0.57	1.80	17.3	0.29	43.4	0.00	1.41	0.88
Max	34.1	5,514	48.1	0.15	0.88	2.26	7.07	58.1	0.88	183	0.01	3.61	2.56
Min	33.0	714	29.9	0.00	0.15	0.61	1.43	0.04	0.02	68.6	BDL	BDL	BDL
Chalcopyrite (n = 6)													
Mean	35.1	3.1	0.06	28.2	0.00	0.00			1.31	0.54	0.01	1.54	1.67
σ	0.6	6.4	0.11	4.3	0.00	0.00			2.06	0.59	0.01	1.51	1.14
Max	35.6	16.1	0.26	34.1	0.01	0.01	BDL	BDL	2.29	1.73	0.02	3.03	3.03
Min	33.9	0.1	0.00	23.8	BDL	BDL	BDL	BDL	0.01	0.21	BDL	BDL	BDL
Sandsloot Reef pyroxenites													
Pyrrhotite (n = 5)													
Mean	38.4	6.47	0.15		1.83	2.87	13.9	0.18	1.32	0.07		1.34	0.48
σ	0.67	2.57	0.02		0.72	0.68	4.43	0.10	1.05	0.07		1.24	0.37
Max	38.8	10.4	0.18	BDL	2.86	3.85	17.3	0.29	2.70	0.16	BDL	3.29	0.92
Min	37.3	3.57	0.12	BDL	1.06	2.22	8.06	0.06	0.09	BDL	BDL	0.15	BDL
Pentlandite (n = 7)													
Mean	35.6	4,398	31.0	0.02	2.02	3.60	15.1	25.1	0.96	102		1.99	0.87
σ	0.22	1,171	2.44	0.02	1.28	1.99	8.94	16.1	0.81	31.1		2.07	0.88
Max	35.2	5,586	32.8	0.04	4.21	5.02	29.3	45.5	2.07	143	BDL	6.14	2.52
Min	35.8	3,068	26.7	BDL	0.64	1.36	4.64	8.20	0.07	67.7	BDL	BDL	BDL
Chalcopyrite (n = 3)													
Mean	34.7	78.6	0.53	30.4	0.03	0.09		0.61	0.12	1.73	0.01	0.22	0.10
σ	0.24	135	0.90	1.42	0.04	0.16		0.62	0.14	2.62	0.01	0.31	0.16
Max	34.8	235	1.57	32.0	0.06	0.27	BDL	1.05	0.28	4.76	0.01	0.44	0.28
Min	34.4	0.07	0.01	29.4	BDL	BDL	BDL	BDL	0.02	0.11	BDL	BDL	BDL
Overysel chromitites													
Pyrrhotite (n = 1)													
	38.8	62.7	0.03	BDL	BDL	BDL	BDL	BDL	BDL	0.03	0.07	0.01	19.7
Pentlandite (n = 1)													
	35.8	5,079	33.7	BDL	0.49	BDL	6.87	BDL	BDL	72.4	BDL	0.81	0.59
Pyrite (n = 2)													
Mean	54.0	127	0.23					0.02		0.19	0.08	1.16	64.9
σ	0.00	122	0.21					0.01		0.08	0.02	1.20	60.8
Max	54.0	213	0.37	BDL	BDL	BDL	BDL	0.02	BDL	0.25	0.09	2.00	108
Min	54.0	40.3	0.08	BDL	BDL	BDL	BDL	0.01	BDL	0.13	0.06	0.31	21.9
Overysel Footwall rocks													
Pyrrhotite (n = 6)													
Mean	39.0	57.1	0.70		0.06	0.11	0.35	0.85	3.34	0.02		1.75	3.97
σ	1.11	23.7	0.21		0.05	0.07	0.33	1.50	4.10	0.03		1.62	4.84
Max	40.0	86.4	1.09	BDL	0.13	0.23	0.82	3.10	9.77	0.08	BDL	2.97	11.1
Min	37.2	39.5	0.47	BDL	0.02	0.04	0.50	BDL	0.01	BDL	BDL	BDL	BDL
Pentlandite (n = 10)													
Mean	33.5	3,144	31.6	0.06	0.03	0.03		0.59	0.45	78.0	0.05	2.81	8.08
σ	1.06	1,239	6.62	0.11	0.03	0.03		0.78	0.63	44.5	0.09	6.20	22.1
Max	36.1	5,184	43.6	0.29	0.07	0.08	BDL	2.04	1.73	170	0.28	18.1	71.0
Min	32.2	788	17.7	BDL	BDL	BDL	BDL	BDL	BDL	28.6	BDL	BDL	0.20

Table 4 continued

	S (wt%)	Co (ppm)	Ni (wt%)	Cu (wt%)	Os (ppm)	Ir (ppm)	Ru (ppm)	Rh (ppm)	Pt (ppm)	Pd (ppm)	Au (ppm)	Te (ppm)	Bi (ppm)
Chalcopyrite (n = 10)													
Mean	34.6	22.7	0.33	27.4	0.00			0.28	0.06	1.71	0.04	0.17	1.13
σ	0.94	52.2	0.67	5.09	0.01			0.22	0.12	1.83	0.05	0.06	1.15
Max	35.4	159	1.84	34.8	0.02	BDL	BDL	0.48	0.32	5.75	0.18	0.25	2.85
Min	32.1	0.10	BDL	19.3	BDL	BDL	BDL	BDL	BDL	0.18	BDL	BDL	BDL
Pyrite (n = 3)													
Mean	53.5	20.9	0.01	0.02					0.03	0.04	0.01	0.43	12.5
σ	0.20	4.31	0.01	0.03					0.05	0.02	0.02	0.27	15.6
Max	53.7	25.0	0.02	0.05	BDL	BDL	BDL	BDL	0.09	0.06	0.03	0.62	23.5
Min	53.3	16.4	BDL	BDL	BDL	BDL	BDL	BDL	BDL	0.03	BDL	BDL	BDL
Limits of detection													
	0.31	0.74	<0.01	<0.01	0.015	0.005	0.067	0.011	0.017	0.034	0.006	0.35	0.84

BDL below detection limit

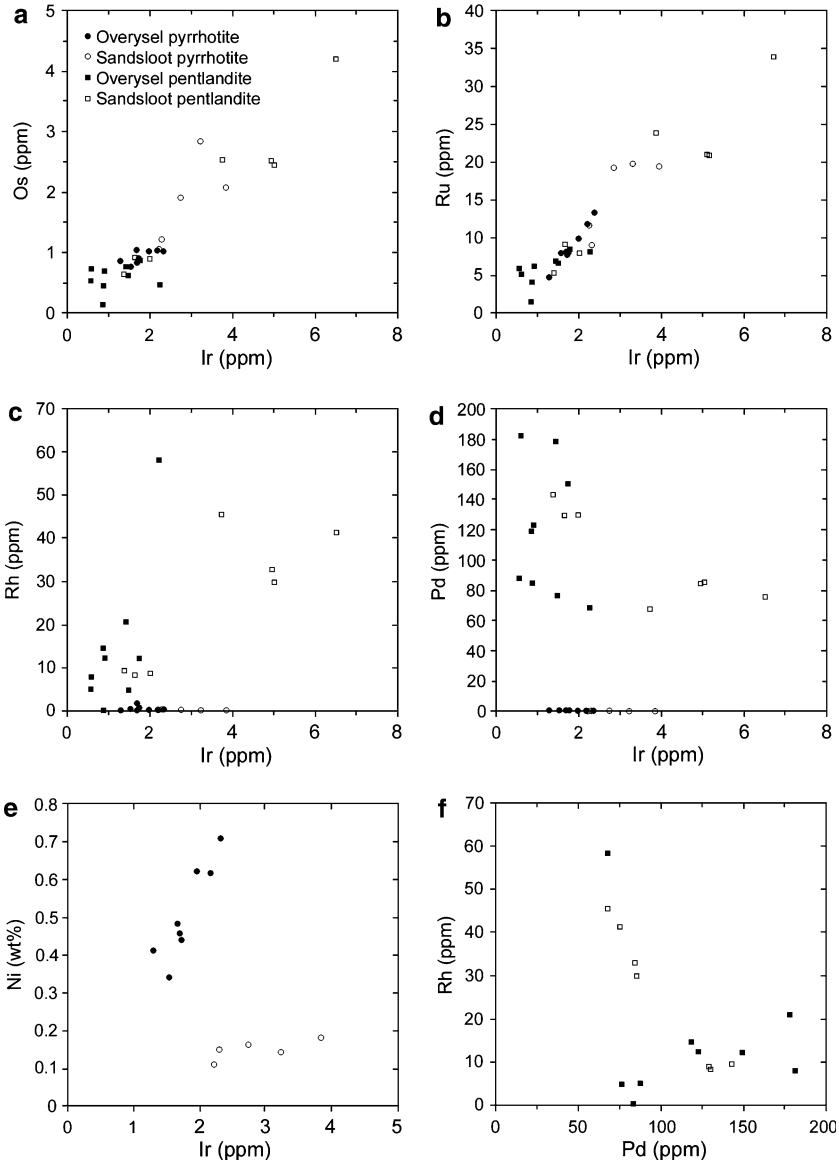

Fig. 4 PGE contents of pyrrhotite and pentlandite grains plotted as **a** Ir versus Os, **b** Ir versus Ru, **c** Ir versus Rh, **d** Ir versus Pd, **e** Ir versus Ni for pyrrhotite and **f** Pd versus Rh for pentlandite

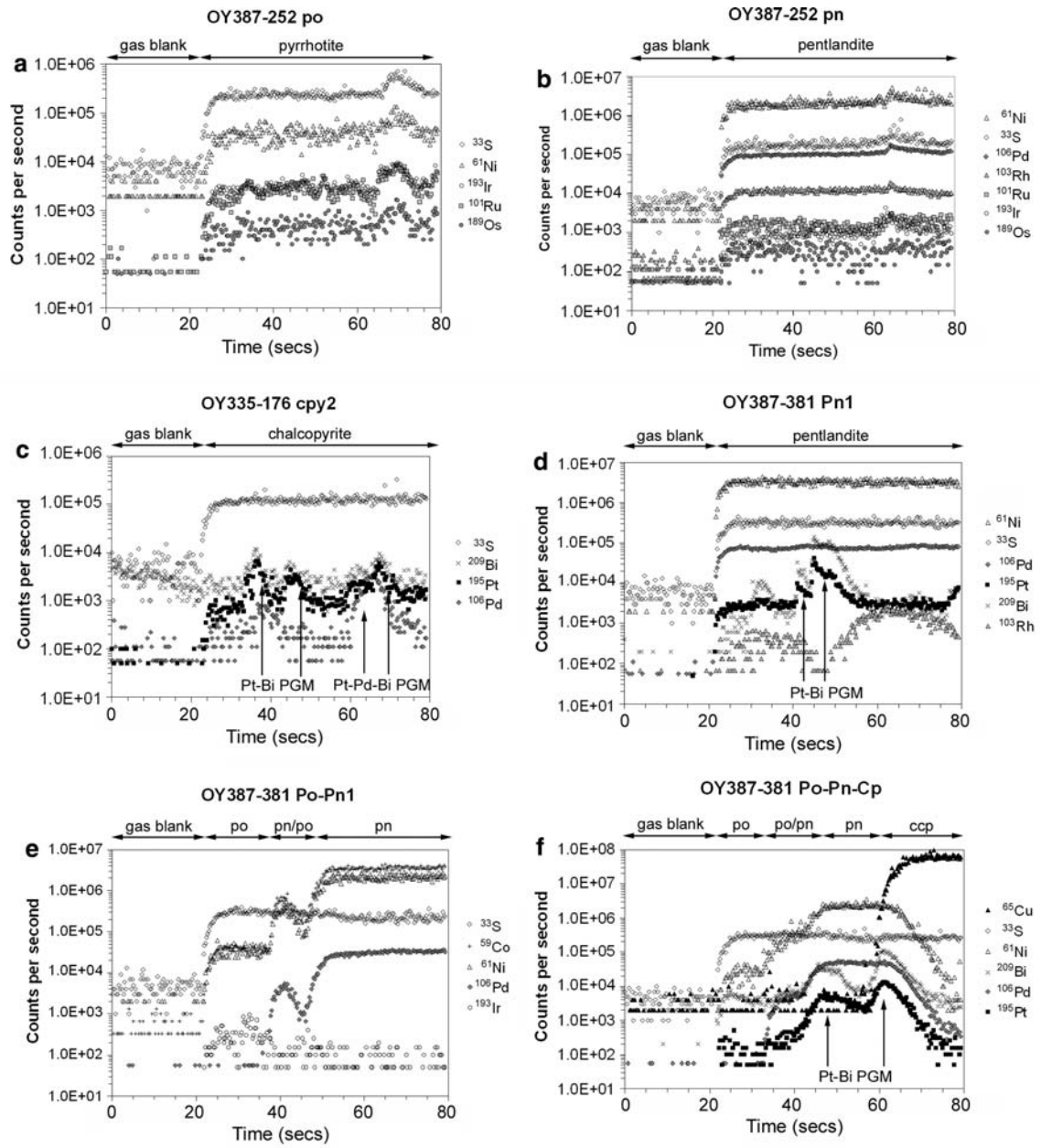

Fig. 5 Selected TRA spectra for **a** pyrrhotite, **b** pentlandite and **c** chalcopyrite with PGM from the Platreef pyroxenites, **d** pentlandite with PGM, **e** composite pyrrhotite–pentlandite, and **f** composite pyrrhotite–pentlandite–chalcopyrite with PGM

The feldspathic pyroxenites from the Platreef at Sandsloot were found to contain consistently higher concentrations of PGE, but almost identical PGE distribution relationships to those at Overysel (Fig. 4a–d, Table 4). Platinum was again present as Bi- and Te-bearing microinclusions in all sulfide phases. Minor Pt was also present (apparently in solid solution) in pyrrhotite and pentlandite in one sample from Sandsloot at concentrations of around 2 ppm (Table 4).

Chromitites

In contrast to the pyroxenitic rocks, the chromitites contain abundant Rh-, Ru- and Ir-bearing PGM (Table 2), and have elevated concentrations of these elements relative to Pt and Pd (Holwell and McDonald 2006). A few sulfide grains were sufficiently large to analyze effectively by laser ablation. One grain of pentlandite, was found to contain no Ir or Rh (Table 4), but did, however, contain some Os and Ru in

comparable concentrations to the pyroxenite-hosted sulfides. This implies that most of the Ir and Rh within the chromitites may be present as PGM, rather than in solid solution in sulfides. A grain of pyrrhotite was also analyzed and found to contain no PGE in solid solution, and was also very low in Ni content.

Footwall gneisses

Holwell and McDonald (2006) showed that there is fractionation of PGE with depth into the gneissic footwall at Overysel, with whole-rock values of Ir, Ru and Rh dropping off dramatically relative to Pt, Pd and Au with increasing depth, and this is reflected in the PGE content of the sulfides. From Table 4 it can be seen that the IPGE content of footwall pyrrhotite and pentlandite is very low, compared to their reef equivalents. Rhodium is present within the pentlandite in variable, but always comparatively low (<2 ppm), concentrations. Whole-rock concentrations of Pt and Pd remain comparable to the reef in mineralized footwall samples. Pentlandite still hosts appreciable amounts of Pd, although to a lesser degree than in the reef, and this is reflected in the greater proportions of Pd-bearing PGM within the footwall rocks compared with the reef pyroxenites (Table 3).

The Pt/Pd ratio in the massive sulfide sample is 0.35, however, virtually all of the PGM found in this sample were Pt phases (Table 2) and there is therefore a case of apparently 'missing' Pd, not represented by any discreet PGM phases. Figure 5d shows a particularly smooth TRA spectrum for a pentlandite from the massive sulfide sample in the footwall (OY387–381), and demonstrates clearly that Pd is present in solid solution. It appears that some Pt is also present in solid solution in low concentrations, but occasional peaks with corresponding Bi peaks indicate the presence of very small Pt–Bi PGM microinclusions as well. The spectrum also shows low concentrations of Rh within the pentlandite, and that a sharp decrease in the Rh signal occurs as the Pt-rich PGM is sampled, indicating a lack of Rh in the PGM phase. Figure 5e illustrates a case where the laser path has passed over pyrrhotite and into pentlandite. The transition can easily be seen by the increase in Ni, as pentlandite is sampled by the laser. This also illustrates the presence of Pd in homogeneous solid solution in pentlandite, and also shows no variation towards the margin of the pentlandite grain. Another polyphase TRA spectrum is shown in Fig. 5f where the laser has sampled firstly pyrrhotite before passing into pentlandite, as seen by the increase in Ni and Pd, and finally chalcopyrite which is shown by the drop in Ni and Pd and the increase in Cu. Two Pt–Bi PGM were sampled, which are labelled on Fig. 5f, which appear to be located at the sulfide grain boundaries. Laser analysis of the exsolution flames of pentlandite in pyrrhotite such as those in Fig. 3e and f shows that the pentlandite flames also contain Pd in solid solution. Chalcopyrite and pyrite in the footwall rocks did not contain any appreciable PGE in solid solution or as microinclusions.

An important relationship in determining the timing of PGE and S saturation in the magma are inclusion relationships in high-temperature cumulus phases. The earliest crystallizing phases in the Platreef at Overysel are chromite, then orthopyroxene. We performed a number of LA-ICP-MS analyses on chromite grains from the chromitite layers, xenoliths and feldspathic pyroxenites, together with several analyses of cumulus orthopyroxenes from the feldspathic pyroxenites. None of the analyses revealed the presence of any PGE, either in solid solution, or as microinclusions, within chromite or orthopyroxene.

Mass balance

For a semi-quantitative indication of the proportions of the PGE present within sulfide minerals and as discreet PGM phases, we adopted a similar approach to the technique used by Ballhaus and Sylvester (2000), in which we recalculate the whole-rock PGE contents to the equivalent in 100% sulfide, and plot the values on a chondrite normalized diagram along with the PGE concentrations of the BMS. As chalcopyrite contains virtually no PGE in solid solution, we recalculate the whole rock PGE contents to 100% pyrrhotite and pentlandite, as these are the two phases, which contain PGE. Including chalcopyrite in the calculations would effectively 'dilute' the PGE content of the calculated sulfide fraction. To improve the technique of Ballhaus and Sylvester (2000), we take into account the different proportions of the sulfide phases present. To calculate this, we adapted the technique described in Huminicki et al. (2005), where all whole-rock Cu and a corresponding amount of S are used to calculate the proportion of chalcopyrite. To improve this further, we used Cu and Ni concentrations obtained by acid leach, which extracts base metals only from the sulfide phase and thus no correction is needed to allow for Ni within silicates, which is necessary if using conventional whole-rock data. The amount of S used in these calculations is based on SEM-EDA analyses of sulfide phases. All whole-rock Ni and a corresponding amount of S are allocated to pentlandite, with the remaining S used to calculate the amount to pyrrhotite. A small correction

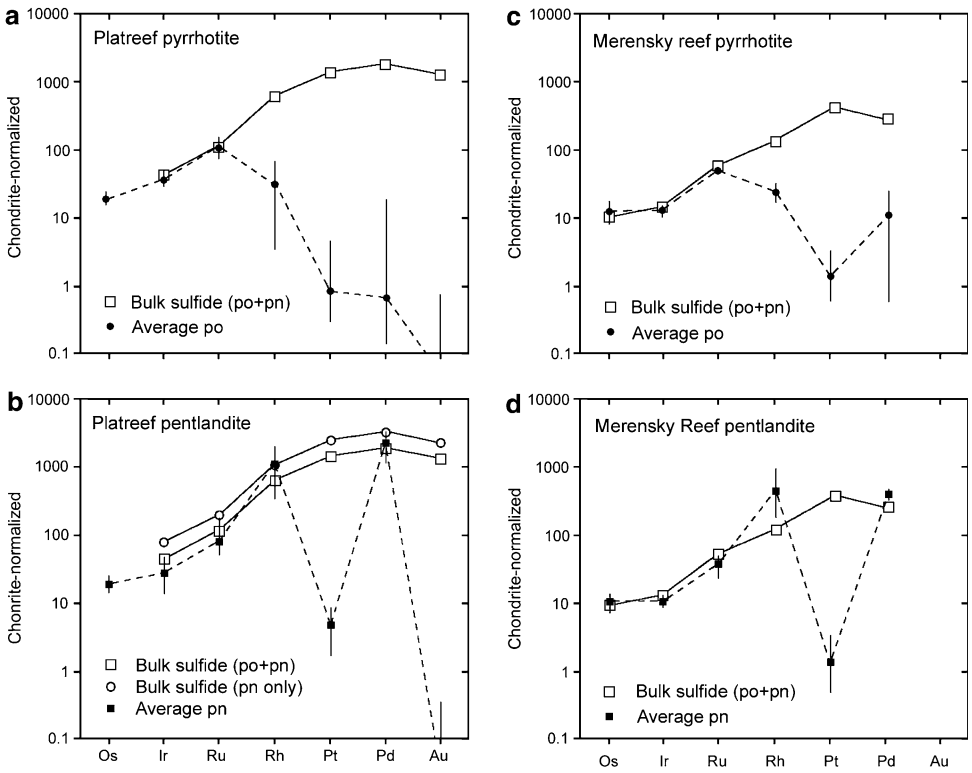

Fig. 6 Chondrite normalized diagrams of average PGE in **a** pyrrhotite and bulk sulfide recalculated to 100% sulfide (po + pn) for Overysel Platreef pyroxenites, and **b** pentlandite and bulk sulfide recalculated to 100% sulfide (po + pn and pn only) for Overysel Platreef pyroxenites, **c** pyrrhotite and bulk sulfide recalculated to 100% sulfide (po + pn) for the Merensky Reef **d** pentlandite and bulk sulfide recalculated to 100% sulfide (po + pn) for the Merensky Reef. Merensky Reef data from Ballhaus and Sylvester (2000)

is made to allow for trace amounts of Ni in pyrrhotite as determined by SEM-EDA analysis. This method does not take into account minor pyrite, however this phase is relatively insignificant volumetrically.

For the pyroxenite samples we analyzed by LA-ICP-MS, we calculated the mean pyrrhotite, pentlandite and chalcopyrite fractions, and then re-calculated the whole-rock concentrations of the PGE and Au to those in 100% sulfide, containing pyrrhotite and pentlandite only. The chondrite normalized values for average PGE contents of pyrrhotite and pentlandite as determined by LA-ICP-MS are plotted with the average whole-rock concentrations for the same samples in Fig. 6a and b together with those calculated for sulfides of the Merensky Reef by Ballhaus and Sylvester (2000), and these are shown in Fig. 6c and d for comparison. The rationale for this method is that an element whose concentration within a sulfide is as high or higher than the bulk value indicates its presence in solid solution, whereas if it falls below, some of that element must be present as discreet phases. It can be seen that the IPGE are comfortably held in solid solution within both pyrrhotite and pentlandite, and Rh and Pd in pentlandite. The slightly higher abundances of Rh and Pd in pentlandite compared to the bulk composition is due to their presence primarily in pentlandite, and thus the bulk rock value is 'diluted' by pyrrhotite that is relatively barren of Rh and Pd (a similar effect on all elements would occur if chalcopyrite were included in the calculations). For this reason we have also plotted the whole-rock values recalculated to 100% pentlandite on Fig. 6b [c.f Fig. 6d, where Ballhaus and Sylvester (2000) did not make this calculation]. Our results show that whole-rock Rh is almost exactly the same as Rh in pentlandite, whereas Pd in pentlandite falls below the whole-rock if recalculated to 100% pentlandite, indicating some Pd-bearing PGM. The large negative anomalies in both Pt and Au show that these are not significantly present in solid solution and must reside in discreet Pt- and Au-bearing phases. These results show that all the IPGE are present in solid solution in pyrrhotite and pentlandite, all Rh and some Pd in solid solution in pentlandite, and they corroborate the PGM studies, which identified 57% of all PGM in the pyroxenites to be Pt phases, 22% electrum and 21% Pd phases (Table 2). From Fig. 6 it can be seen that our data from the Platreef show remarkable similarities to that for the Merensky Reef sulfides, which would suggest that the sulfides in both deposits were enriched in PGE at an early stage and underwent a similar cooling history.

Discussion

This study into the PGM mineralogy of the Platreef at Overysel has revealed characteristic PGM assemblages

and associations in different lithologies, which are dominated by Pt and Pd phases. The LA-ICP-MS study has not only identified the major carriers of the IPGE and Rh in the Platreef to be pyrrhotite and pentlandite, but also provides an insight into the partitioning behaviour of the individual PGE during crystallization of a sulfide liquid and also reveals the processes involved in the enrichment of noble metals in the Platreef.

The role of a sulfide liquid in Platreef PGE mineralization

The chalcophile nature of the PGE is well known and, in the presence of a sulfide liquid, the high distribution coefficients (D) of the PGE between sulfide and silicate melts mean that they will be effectively collected by any sulfide liquid separating from a silicate magma. There have been several studies into the Fe–Ni–Cu–S system, which have been used to assess the partitioning of PGE during the crystallization of monosulfide solid solution (mss) from a sulfide liquid (e.g., Fleet et al. 1993; Li et al. 1996; Barnes et al. 1997; Ballhaus et al. 2001; Mungall et al. 2005). Their data are summarized in Table 5 and show that D_{Pt}, D_{Pd} and D_{Au} are all <1 and these elements are therefore concentrated in the residual liquid during mss crystallization. D_{Os}, D_{Ir} D_{Ru} and D_{Rh} are all much >1 in S-rich systems and partition into mss. The partitioning is particularly affected by varying fS_2 conditions and the compatibility in mss of these elements decreases as the S-content of the liquid decreases, so that in very S-poor, alloy-dominant systems, only Ru remains compatible in mss. As the Platreef is relatively S-rich, the PGE in a sulfide liquid within the Platreef should behave in the manner expected from the experimental results during the crystallization of mss. Holwell and McDonald (2006) demonstrated that PGE were originally present in a sulfide liquid within the Platreef magma, which cooled to form the observed pyrrhotite–pentlandite–chalcopyrite–PGM assemblage. Our LA-ICP-MS analyses of the sulfide phases and the complementary PGM studies can, therefore, be used to compare the natural partitioning behaviour in the Platreef with that expected from the experimental results.

Using the experimentally derived partitioning data, one would expect the IPGE and Rh to be enriched in mss, and to be present in solid solution within its cooling products: pyrrhotite and pentlandite, and this is precisely what is observed in our LA-ICP-MS analyses. The IPGE were concentrated in early crystallizing mss, which on cooling exsolves to Fe–mss and Ni–mss, then to pyrrhotite and pentlandite (Barnes et al. 2006), with the IPGE remaining in solid solution. The enrichment of the IPGE in pyrrhotite compared to pentlandite (1.5 times) may indicate a slight preference for these elements to partition into pyrrhotite during the exsolution process. A similar relationship was also found to be present in the sulfides of the Merensky Reef, where Ballhaus and Sylvester (2000) noted the IPGE to be about 1.2 times more enriched in pyrrhotite than pentlandite, although this is not necessarily a consistent relationship, as seen by the contrasting concentrations in the Sandsloot samples and Barnes et al. (2006) found broadly similar IPGE concentrations in pyrrhotite and pentlandite in their LA-ICP-MS study on sulfides from Noril'sk. Rhodium is also compatible in mss, however it is present only in pentlandite in our samples, and therefore during the exsolution process it appears that Rh preferentially partitions into the Ni-rich mss which forms pentlandite on cooling.

According to the experimental studies, after crystallization of mss, Pt, Pd and Au should be concentrated in the residual sulfide liquid which will crystallise intermediate solid solution (iss), which on cooling exsolves to chalcopyrite plus pentlandite. Peregoedova (1998) showed experimentally that Pt and Pd (and by implication, Au) are also incompatible in iss. However, some Pd is present in solid solution in pentlandite in significant amounts (up to 180 ppm, Table 4) and the presence of Pd within the pentlandite exsolution flames in pyrrhotite such as those shown in Fig. 3e and f implies that some Pd is likely to have been present in mss.

Fleet et al. (1993) included minor amounts of As, Bi and Te, which are also highly chalcophile at magmatic temperatures and are among the most common ele-

Table 5 Experimentally derived partition coefficients for the noble metals between monosulfide solid solution and sulfide liquid (900–1200°C)

Os	Ir	Ru	Rh	Pt	Pd	Au	Reference
4.3	3.6	4.2	3.0	0.2	0.2	0.09	Fleet et al. (1993)
	1.1–13		0.047–8.3	0.05–0.16	0.08–0.27		Li et al. (1996)
	0.43–17		0.045–7.43	0.013–0.46	0.005–0.44		Barnes et al. (1997)
5	3.1–11.8	3–19	1.5–3.5	0.017–0.13	0.058–0.19		Ballhaus et al. (2001)
	4.55–7.68	8.71–13.5	3.45–5.66	0.035–0.052	0.072–0.12	0.006–0.013	Mungall et al. (2005)

ments to form PGM with Pt and Pd. They found that during quenching, Bi, Te and As segregate as a late residual liquid which scavenges Pt preferentially over Pd. Helmy et al. (2006) performed experiments in sulfide–telluride systems and found that telluride (and bismuthide and antimonide) melt is immiscible in sulfide melt below temperatures of 1,000°C. Furthermore, telluride melt remains liquid after the sulfide solidus and that Pt and Pd strongly partition into this melt. They also noted that Pt and Pd are more strongly complexed with Te and Bi than S, and Pd will only enters mss when the Pd/semi metal ratio is sufficiently high to have an excess of Pd that cannot be accommodated by the telluride/bismuthide melt. Therefore a high Pd/semi metal ratio can explain the presence of Pd in pentlandite in our samples. These observations by Helmy et al. (2006) seem to substantiate the theories of Cabri and Laflamme (1976), Prichard et al. (2004) and Barnes et al. (2006) who all suggested that Pt, Pd and Au along with semi metals such as Bi, Te, As and Sb are concentrated in a late-stage residual melt after the crystallization of iss that is expelled to the grain boundaries. Subsequent crystallization of this liquid then forms PGM around the margins of the sulfide blebs and in small veinlets injected into the surrounding silicates, which explains the tendency for PGM to be present around the margins of sulfide blebs as seen by over half of the PGM in the reef pyroxenites being hosted by primary silicates around the margins of the BMS grains. Later alteration of the sulfide blebs, with replacement by secondary amphiboles around the margins of BMS blebs, appears not to affect the early-formed PGM, which are then isolated as satellite grains within secondary silicates around the BMS blebs as is shown in Fig. 3a.

The case of the Pt–Bi–Te microinclusions within all sulfides is interesting as it infers that Pt and Bi were present in both mss and iss. It is unlikely that they exsolved from the sulfide liquid as exsolution tellurides/bismuthides have characteristically high Ni contents, which our tellurides/bismuthides do not. Platinum is also incompatible in both mss and iss, however it is highly compatible in telluride and bismuthide melt, which is immiscible in sulfide melt below 1,000°C (Helmy et al. 2006). We suggest that the microinclusions represent minute droplets of this immiscible melt that remained trapped within crystallising mss and iss, and failed to be expelled to the grain boundaries to form the satellite PGM grains as described above. This also implies Bi and Te were present within the initial sulfide liquid. The footwall gneisses also display a similar BMS–Pt/Pd telluride assemblage and it is assumed that these assemblages formed directly from the crystallization of a sulfide melt in a similar manner, as concluded by Holwell and McDonald (2006).

Hutchinson and McDonald (2005) presented some initial results for Pt and Pd in sulfides from a LA-ICP-MS study on the Platreef at Turfspruit (Fig. 1). They also found that Pt was not present in solid solution in any of the sulfide phases, but was present as Pt–Pd–Bi microinclusions within all phases. Palladium was found to be present erratically in pentlandite, but more commonly as PGM inclusions, and the overall abundances of the IPGE within the sulfides was much lower than at Overysel (Hutchinson and McDonald, unpublished data). Hutchinson and McDonald (2005) attributed the absence of PGE within sulfides to the degree of contamination from assimilated footwall rocks (e.g., Sharman-Harris et al. 2005), which also introduced elements such as As, Sb, Bi and Te. As a consequence, the PGE (particularly Pt and Pd) effectively formed PGM with these elements which were either not collected by the sulfide liquid, or were expelled from them during crystallization. The partial melting of the floor on Overysel is thought to post-date the mineralization (Barton et al. 1986) and is unlikely to have released similar concentrations of volatile elements as the sedimentary floor at Turfspruit. Our data implies that that Bi and Te were present within the mineralizing sulfide liquid, and that local contamination at Turfspruit served to the increase the amounts of semi metals, particularly Sb and As, in that area which resulted in a higher volume of immiscible semi metal rich melt, restricting the amount of PGE that partitioned into the sulfides.

Hydrothermal effects on PGM mineralogy

The most unaltered PGM assemblages in the Platreef appear to be the sulfide-associated telluride and chromite-associated laurite-dominant assemblages. All others are likely to be secondary: either modified from the original telluride-dominant one, or ones related to transport by a hydrothermal fluid. The serpentinized calc-silicate xenoliths show a distinctive assemblage, dominated by sperrylite, with some bismuthides, hollingworthite and Pd tellurides. The presence of sperrylite in calc-silicate footwall rocks at Sandsloot is common, as is the presence of Pd tellurides in serpentinized footwall rocks, and these associations are thought to be characteristic of hydrothermal transport of PGE (Holwell et al. 2006). The presence of Rh-bearing PGM is also suggestive of a secondary assemblage as all Rh appears to be sufficiently held in solid solution within pentlandite in the unaltered assem-

blages. The associations are also dominantly silicate associated, which is indicative of volatile activity (e.g., Holwell et al. 2006). It is unlikely that PGE were present in the original protolith, so introduction of PGE into the xenolith is likely to have been related to fluid activity associated with either metamorphism, syn- to post-intrusion or serpentinization after intrusion and xenolithization. The amphibolitized gneisses associated with the intrusion of late-stage granitic dykes have a more Pt-dominant assemblage which may be due to the more mobile Pd being transported away by the fluids associated with the alteration.

The bleached appearance and presence of hydrous minerals in the mineralized basement granite would suggest that the assemblage is the product of either a hydrothermal modification of an assemblage similar to that in the gneisses, or a hydrothermal halo at the base of the mineralized zone. Farrow and Watkinson (1997) describe almost identical sulfide assemblages containing chalcopyrite and millerite associated with Bi-bearing PGM such as sobolevskite, froodite and michenerite in the alteration zones around the Cu-rich veins at the deepest extremities of the mineralized zones at Sudbury, which they estimate to have formed at around 200–300°C. It is likely that the strikingly similar assemblage in the granite in borehole OY387 was formed by the expulsion of a hydrothermal fluid from the final stages in the evolution of the migrating sulfide liquid, analogous to that postulated for Sudbury by Li and Naldrett (1993). The assemblage in the thin Lower Zone-like pyroxenite may be of similar origin as it contains abundant bismuthides, associated with a chalcopyrite-dominant BMS assemblage. This contrasts with the Ni-rich magmatic sulfides that might be expected in such rocks if the sulfide were of a magmatic origin (c.f. the Lower Zone-hosted Volspruit deposit, Hulbert and von Gruenewaldt 1982; Harmer 2004).

Chromitites and the timing of S saturation

Inclusion relationships, and in particular the presence of PGM microinclusions, have been used as an important indicator of the processes involved in noble metal enrichment in magmatic PGE deposits. Ballhaus and Sylvester (2000) identified PGM microinclusions within chromite and olivine in the Merensky Reef and suggested that they formed from the development of PGE clusters (as proposed by Tredoux et al. 1995) in the magma, prior to collection by early crystallizing phases in the magma. The lack of such PGM microinclusions in high-temperature cumulus phases in the Platreef may imply that sulfur saturation and collection of PGE and semi metals by the resultant sulfide droplets occurred prior to the crystallization of any cumulus phases. If so, it is possible that when the Platreef magma was intruded it already contained preformed sulfide droplets, such as in the model of Lee (1996), who suggested the PGE-rich sulfides were preconcentrated in a deep staging chamber. In such a case, the mass balance problem of the large volume of magma needed to be processed to extract the volumes of PGE present in the Platreef (e.g., Cawthorn et al. 1985; Cawthorn et al. 2002), which is imposed by the late intrusion of Main Zone rocks (Holwell et al. 2005; Holwell and Jordaan 2006) can be resolved.

In our chromitite samples, the PGM assemblage is dominated by minerals containing the IPGE and Rh, which is typical of chromite-associated PGE deposits. The presence of laurite with chromite, especially as inclusions, is considered to be of magmatic origin in chromite ores (Bockrath et al. 2004) and the behaviour of Ru is an important indicator of fS_2 conditions within a silicate magma. Laurite and Ru–Os–Ir alloy form under conditions of sulfur-undersaturation (Brenan and Andrews 2001), and therefore the presence of inclusions of these phases within primary liquidus phases such as chromite would suggest that early crystallization took place in sulfide-undersaturated conditions. Additionally, Bockrath et al. (2004) showed experimentally that, although thermodynamically, laurite can be a liquidus phase that crystallizes directly from a sulfide-undersaturated magma, many grains of laurite may be 'secondary', although still magmatic. Their experiments showed that Ru metal nucleates on the surfaces of chromite grains, and that later reaction between Ru and S following an increase in fS_2 forms laurite. In either of the above cases, the presence of laurite is indicative of sulfur-undersaturated conditions at the time of chromite precipitation. This common association in the Overysel chromitites of laurite on the surfaces of chromite grains may imply that the chromitites crystallized under conditions of S undersaturation, however very few were found as inclusions and no Ru–Os–Ir alloy was found.

If sulfur-saturation occurs concurrently with, or prior to, the earliest crystallizing phases, laurite and Ru–Ir–Os alloy will not form and the IPGE will partition into mss (Brenan and Andrews 2001). There are no records of Ru–Ir–Os alloy in the Platreef and, with the exception of the chromitites described here laurite, is also very rare (Kinloch 1982; Armitage et al. 2002; Hutchinson and Kinnaird 2005; Holwell et al. 2006). It is possible that chromite precipitation occurred at a similar time to S saturation with laurite and hollingworthite forming with chromite at high temperatures (hollingworthite is stable to at least 850°C, Makovicky

2002). However, given the relatively volumetric insignificance of chromite, this still allowed for appreciable amounts of the IPGE and Rh to be scavenged by the sulfide liquid.

Comparison with other Platreef localities and economic implications

The dominance of Pt and Pd tellurides and bismuthotellurides in the Platreef pyroxenites is common throughout the Platreef (Viljoen and Schürmann 1998; Hutchinson and Kinnaird 2005; Holwell et al. 2006). Hutchinson and Kinnaird (2005) attributed the mineralogy of the PGM at Turfspruit, which is dominated by tellurides, antimonides and bismuthides, to be a result of the incorporation of S, As, Te, Bi and Sb into the Platreef magma from devolatilization of Duitchland Formation floor rocks. However, whilst this may be the case with Sb and As (antimonides and arsenides are very rare at Overysel), the ubiquity of Te and Bi along strike may suggest its presence in the Platreef sulfide was derived before emplacement, rather than as a local addition from floor rocks.

The major contrasts between Overysel and the areas to the south are the presence of PGE sulfides and paucity of antimonides and alloys at Overysel. Work by Armitage et al. (2002) and Holwell et al. (2006) have shown that fluid activity has exercised a considerable influence on the resulting mineralogy, distribution and BMS association of the PGE, particularly into the footwall at Sandsloot, with all of the antimonide and alloy dominated assemblages at Sandsloot occurring within rocks that have been subjected to significant fluid activity related. Such volatile activity is more uncommon at Overysel, except within and around calc-silicate xenoliths, and the extent of hydrothermal activity is governed by a fundamental footwall control. The dolomite floor at Sandsloot released large volumes of fluids during assimilation and metamorphism, and subsequent serpentinization, whereas the largely anhydrous gneissic footwall at Overysel produced few volatiles. As a result of the lack of hydrothermal redistribution at Overysel, the PGE telluride–BMS association observed in the pyroxenites at this locality appear to be the most ‘primary’ mineralization style preserved, in terms of it being unaltered by fluids, and being a direct result of the in situ cooling of a sulfide liquid. The ubiquity of this assemblage to varying degrees all along strike indicates a common initial mineralization style, but also that hydrothermal redistribution is highly variable along strike.

This study has revealed that the Platreef at Overysel preserves a mineralization style that is the product of the fractional crystallization of a sulfide liquid within the Platreef magma. Pyrrhotite and pentlandite host virtually all of the bulk Os, Ir and Ru. Virtually all the bulk Rh and some Pd is hosted by pentlandite, whereas virtually all Pt and Au, and some Pd form discreet PGM that are in close spatial association with BMS. This knowledge has obvious implications for exploration and for mineral processing. More important is the identification that extensive hydrothermal activity disrupts this assemblage by redistributing the PGE, changing the mineralogy, and often decoupling the PGE–BMS association. The amount of hydrothermal activity is fundamentally controlled by footwall lithology and for this reason, in different areas of the Platreef (and by implication other basal PGE–BMS deposits, where the assimilation of reactive footwall rocks has been extensive) the ‘classic’ primary associations are less likely to hold true throughout the reef. As a result, exploration for, and recovery of, ore in such areas may suffer without detailed mineralogical investigations.

Conclusions

This combined PGM and LA-ICP-MS study has revealed the complex behaviour of the PGE during Platreef mineralization. A sulfide liquid originally concentrated PGE and semi metals such as Bi and Te in the Platreef magma at an early stage, before the crystallization of cumulus orthopyroxene, but concurrently with chromite. This may have occurred in a deep staging chamber or conduit prior to intrusion. During post-intrusion crystallization of the sulfide, IPGE and Rh partitioned into early crystallizing mss, which on further cooling exsolved to pyrrhotite and pentlandite, with the IPGE remaining in solid solution within both phases and Rh partitioning preferentially into pentlandite. Virtually all Pt, Au and some Pd was concentrated with semi metals in a late stage melt with some excess Pd partitioning into Ni-rich mss. This immiscible semi metal rich melt cooled to form PGM around the margins of the sulfide blebs. Tiny droplets trapped in the crystallized mss and iss formed PGM microinclusions. Some secondary redistribution by minor hydrothermal activity has occurred in and around xenoliths, and in the deepest zones of footwall mineralization, which typically form more bismuthide-dominated PGM assemblages and have led to some decoupling of PGM from sulfide minerals. Overall, however, the lack of hydrothermal interaction and overprinting compared to that observed in areas where sediments form the immediate footwall raises the possibility that the

Platreef at Overysel represents the most 'primary' style of Platreef mineralization. As such, the Platreef can be considered to be primarily an orthomagmatic PGE–Cu–Ni sulfide deposit.

Acknowledgments The authors would like to thank the management of Anglo Platinum for giving permission to publish this work, and for allowing access to core from Overysel and to the Sandsloot mine. David Holwell's Ph.D. research is funded by the Natural Environment Research Council and supported by Anglo Platinum through Industrial CASE project (NER/S/C/2003/11952). Thanks to Jay Cockayne for proof reading the manuscript and constructive reviews by Chris Ballhaus and an anonymous referee are greatly acknowledged in improving the quality and focus of the manuscript.

References

Armitage PEB, McDonald I, Edwards SJ, Manby GM (2002) Platinum-group element mineralization in the Platreef and calc-silicate footwall at Sandsloot, Potgietersrus District, South Africa. Appl Earth Sci (Trans Inst Min Metall B) 111:B36–B45

Ballhaus C, Sylvester PJ (2000) Noble metal enrichment processes in the Merensky Reef, Bushveld Complex. J Petrol 41:545–561

Ballhaus C, Tredoux M, Späth A (2001) Phase relations in the Fe–Ni–Cu–PGE–S system at magmatic temperature and application to massive sulphide ores of the Sudbury igneous complex. J Petrol 42:1911–1926

Barnes S-J, Makovicky E, Makovicky M, Rose Hansen J, Karup Moller S (1997) Partition coefficients for Ni, Cu, Pd, Pt, Rh and Ir between monosulfide solid solution and sulfide liquid and the formation of compositionally zoned Ni–Cu sulfide bodies by fractional crystallization of a sulfide liquid. Can J Earth Sci 34:366–374

Barnes S-J, Cox RA, Zientek ML (2006) Platinum-group element, gold, silver and base metal distribution in compositionally zoned sulfide droplets from the Medvezky Creek Mine, Noril'sk, Russia. Contrib Mineral Petrol 152:187–200

Barton Jr JM, Cawthorn RG, White J (1986) The role of contamination in the evolution of the Platreef of the Bushveld Complex. Econ Geol 81:1096–1104

Bockrath C, Ballhaus C, Holzheid A (2004) Stabilities of laurite RuS_2 and monosulfide liquid solution at magmatic temperature. Chem Geol 208:265–271

Brenan JM, Andrews D (2001) High-temperature stability of laurite and Ru–Os–Ir alloy and their role in PGE gractionation in mafic magmas. Can Mineral 39:341–360

Cabri LJ, Laflamme JHG (1976) The mineralogy of the platinum-group elements from some copper–nickel deposits of the Sudbury area, Ontario. Econ Geol 71:1159–1195

Cabri LJ, Sylvester PJ, Tubrett MN, Peregoedova A, Laflamme JHG (2003) Comparison of LAM-ICP-MS and Micro-PIXE results for palladium and rhodium in selected samples of Noril'sk and Talnakh sulfides. Can Mineral 41:321–329

Cawthorn RG, Barton Jr JM, Viljoen MJ (1985) Interaction of floor rocks with the Platreef on Overysel, Potgietersrus, Northern Transvaal. Econ Geol 80:988–1006

Cawthorn RG, Merkle RKW, Viljoen MJ (2002) Platinum-group elements in the Bushveld Complex. In: Cabri LJ (ed) The geology, geochemistry, mineralogy and mineral benificiation of platinum-group elements. Can Inst Min Metall Petroleum, special vol 54. pp 389–430

Council for Geoscience (1995) Pietersburg. Geological Survey of South Africa 1:250,000 Metallogenic Series, 2328

Eales HV, Cawthorn RG (1996) The Bushveld Complex. In: Cawthorn RG (ed) Layered intrusions. Elsevier, Amsterdam, pp 181–230

Farrow CEG, Watkinson DH (1997) Diversity of precious-metal mineralization in footwall Cu–Ni–PGE deposits, Sudbury, Ontario: implications for hydrothermal models of formation. Can Mineral 35:817–839

Fleet ME, Chryssoulis SL, Stone WE, Weisener CG (1993) Partitioning of platinum-group elements and Au in the Fe–Ni–Cu–S system: experiments on the fractional crystallization of sulfide melt. Contrib Mineral Petrol 115:36–44

Harmer RE (2004) The Volspruit PGE–Ni reef: platinum mineralization in the Lower Zone south of Mokopane. Geoscience Africa 2004, abstract vol. Univ Witwatersrand, Johannesburg, pp 256–257

Helmy HM, Ballhaus C, Berndt J, Bockrath C, Wohlgemuth-Ueberwasser C (2006) Formation of Pt, Pd and Ni tellurides: experiments in sulfide–telluride systems. Contrib Mineral Petrol DOI 10.1007/s00410-006-0163-7

Holwell DA, Jordaan A (2006) Three-dimensional mapping of the Platreef at the Zwartfontein South mine: implications for the timing of magmatic events in the northern limb of the Bushveld Complex South Africa. Appl Earth Sci (Trans Inst Min Metall) 115:41–48

Holwell DA, McDonald I (2006) Petrology, geochemistry and the mechanisms determining the distribution of platinum-group element and base metal sulfide mineralization in the Platreef at Overysel, northern Bushveld Complex, South Africa. Mineral Deposita 41:575–598

Holwell DA, Armitage PEB, McDonald I (2005) Observations on the relationship between the Platreef and its hangingwall. Appl Earth Sci (Trans Inst Min Metall) 114:199–207

Holwell DA, McDonald I, Armitage PEB (2006) Platinum-group mineral assemblages in the Platreef at the South Central Pit, Sandsloot Mine, northern Bushveld Complex, South Africa. Mineral Mag 70:83–101

Hulbert LJ, von Gruenewaldt G (1982) Nickel, copper and platinum mineralization in the Lower Zone of the Bushveld Complex, south of Potgietersrus. Econ Geol 77:1296–1306

Huminicki MAE, Sylvester PJ, Cabri LJ, Lesher CM, Tubrett M (2005) Quantitative mass balance of platinum group elements in the Kelly Lake Ni–Cu–PGE deposit, Copper Cliff Offset, Sudbury. Econ Geol 100:1631–1646

Hutchinson D, Kinnaird JA (2005) Complex multi-stage genesis for the Ni–Cu–PGE mineralization in the southern region of the Platreef, Bushveld Complex, South Africa. Appl Earth Sci (Trans Inst Min Metall B) 114:B208–B224

Hutchinson D, McDonald I (2005) Breaking the rules. Divergent behaviour of platinum and palladium in the northern limb of Bushveld Complex, R.S.A. In: Törmänen TO, Alapieti TT (eds) 10th International Platinum Symposium, Ext Abstracts, pp 118–121

Hutchinson D, McDonald I (2006) Formation of high-temperature Pt–arsenides and antimonides and their subsequent expulsion from sulphide liquids. A case study by laser ablation ICP-MS from the Northern Limb of the Bushveld Complex, R.S.A. Mineral Deposita (in press)

Kendall T (2006) Platinum 2006. Johnson Matthey, Royston, p 52

Kinloch ED (1982) Regional trends in the platinum-group mineralogy of the Critical Zone of the Bushveld Complex, South Africa. Econ Geol 77:1328–1347

Kinnaird JA, McDonald I (2005) An introduction to mineralisation in the northern limb of the Bushveld Complex. Appl Earth Sci (Trans Inst Min Metall B) 114:B194–B198

Lee CA (1996) A review of mineralization in the Bushveld Complex and some other layered mafic intrusions. In: Cathorn RG (ed) Layered intrusions. Elsevier, Amsterdam, pp 103–146

Li C, Naldrett AJ (1993) Platinum-group minerals from the Deep Copper Zone of the Strathcona deposit, Sudbury, Ontario. Can Mineral 31:31–44

Li C, Barnes S-J, Makovicky E, Rose-Hansen J, Makovicky M (1996) Partitioning of nickel, copper, iridium, rhenium, platinum and palladium between monosulfide solid solution and sulfide liquid: effects of composition and temperature. Geochim Cosmochim Acta 60:1231–1238

Makovicky E (2002) Ternary and quaternary phase systems with PGE. In: Cabri LJ (ed) The geology, geochemistry, mineralogy and mineral benificiation of platinum-group elements. Can Inst Min Metall Petroleum, special vol 54, pp 131–175

McDonald I (2005) Development of sulfide standards for the in-situ analysis of platinum-group elements by laser ablation inductively coupled plasma-mass spectrometry (LA-ICP-MS). In: Törmänen TO, Alapieti TT (eds) 10th International Platinum Symposium, Ext Abstracts, pp 468–471

Mungall JE, Andrews DRA, Cabri LJ, Sylvester PJ, Tubrett M (2005) Partitioning of Cu, Ni, Au, and platinum-group elements between monosulfide solid solution and sulfide melt under oxygen and sulfur fugacities. Geochim Cosmochim Acta 69:4349–4360

Peregoedova AV (1998) The experimental study of the Pt–Pd–partitioning between monosulfide solid solution and Cu–Ni–sulfide melt at 900–840°C. In 8th International Platinum Symposium abstracts. Geol Soc South Africa and South African Inst Min Metall, Symposium Series, S18:325–373

Prichard HM, Hutchinson D, Fisher PC (2004) Petrology and crystallization history of multiphase sulfide droplets in a mafic dike from Uruguay: implications for the origin of Cu–Ni–PGE sulfide deposits. Econ Geol 99:365–376

Sharman-Harris ER, Kinnaird JA, Harris C, Horstmann UE (2005) A new look at sulphide mineralisation of the northern limb, Bushveld Complex: a stable isotope study. Appl Earth Sci (Trans Inst Min Metall B) 114:B252–263

Tredoux M, Lindsay NM, Davies G, McDonald I (1995) The fractionation of platinum-group elements in magmatic systems, with the suggestion of a novel causal mechanism. S Afr J Geol 98:137–167

Viljoen MJ, Schürmann LW (1998) Platinum group metals. In: Wilson MGC, Anhaeusser CR (eds) The mineral resources of Southern Africa. Council for Geoscience, pp 532–568

White JA (1994) The Potgietersrus prospect—geology and exploration history. XVth CMMI Congress, Johannesburg, SAIMM, vol 3, pp 173–181